Optics and Lasers in Engineering 47 (2009) 865–874

Contents lists available at ScienceDirect

Optics and Lasers in Engineering

journal homepage: www.elsevier.com/locate/optlaseng

Digital image correlation using iterative least squares and pointwise least squares for displacement field and strain field measurements

Bing Pan [a,b,*], Anand Asundi [a], Huimin Xie [b], Jianxin Gao [c]

[a] School of Mechanical and Aerospace Engineering, Nanyang Technological University, 639798 Singapore, Singapore
[b] FML, Department of Engineering Mechanics, Tsinghua University, Beijing 10084, China
[c] The Welding Institute, Great Abington, Cambridge CB21 6AL, UK

ARTICLE INFO

Article history:
Received 15 September 2008
Received in revised form
21 October 2008
Accepted 21 October 2008
Available online 20 February 2009

Keywords:
Digital image correlation
Deformation
Iterative least squares
Pointwise least squares

ABSTRACT

Digital image correlation (DIC) method using iterative least squares algorithm (ILS) for displacement field measurement and pointwise least squares algorithm (PLS) for strain field measurement is proposed in this paper. A more general and practical intensity change model is employed with consideration of the linear intensity change of the deformed image, followed by an iterative least squares algorithm for calculating displacement field with sub-pixel accuracy. The concept of correlation function is not used in the ILS method, even though we prove that the algorithm is actually equivalent to the optimization of the sum of squared difference correlation function using improved Newton–Raphson method. Besides, different from the conventional strain estimation approaches based on smoothing the displacement fields first and followed by differentiation of the smoothed displacement fields, a simple yet effective PLS algorithm is proposed for extracting strain fields from the computed displacement fields. The effectiveness and accuracy of the proposed techniques is verified through numerical simulation experiments. A practical application of the algorithms to residual plastic deformation field measurement of GH4169 alloy subjected to tensile fatigue is also presented.

1. Introduction

Digital image correlation (DIC) is a practical and effective optical technique for surface deformation measurement. By processing the digital images of a test object surface recorded by an imaging device (typically a CCD camera) before and after deformation, DIC directly provides full-field displacements of the object surface to sub-pixel accuracy, and strains can be calculated directly or by further manipulations of the displacement fields. Due to its advantages of simple experimental set-up and specimen preparation, low requirements on measurement environment and flexible measurement sensitivity and resolution, DIC has been widely used for full-field deformation measurement in the field of experimental mechanics.

The basic principle of DIC is to match (or track) the same physical points imaged in the reference image and the deformed image. To this end, a square subset surrounding the interrogated point in the reference image is selected and used to find its corresponding location in the deformed image. Normally, certain correlation criterion should be defined in advance to evaluate the similarity degree between the reference subset and its target subset. Due to the discrete nature of digital images, integer pixel displacements of the subset can be easily computed by implementing simple searching scheme within the deformed image. To further improve the accuracy of DIC, certain kind of sub-pixel registration algorithm should be used [1]. Various sub-pixel registration algorithms have been proposed in literature. Among them the iterative spatial domain cross-correlation algorithm using Newton–Raphson (NR) [2] or improved NR method [3–6] are widely recognized as one of the optimal approaches and highly recommended for practical use due to its measurement accuracy and computational efficiency. However, calculation of second-order derivatives of correlation function (i.e., Hessian matrix) is required in NR algorithm, which greatly increases the computational complexity. An important improvement to NR method was made by Vendroux and Knauss [3] with an approximation to the Hessian matrix, through which the computation complexity was decreased without loss of accuracy.

To avoid the computational complexity and burden involved in the optimization of correlation function using NR method, another technique for accurate sub-pixel displacement measurement is the iterative spatial-gradient-based method proposed by Zhou and Goodson [7]. In fact, this algorithm was originally introduced from optical flow method [8], which simply assumes the intensity of the same physical point on the test object surface shall remain constant in the images captured at different time. Since it only

* Corresponding author.
E-mail address: panb04@mails.tsinghua.edu.cn (B. Pan).

0143-8166/$ - see front matter © 2009 Elsevier Ltd. All rights reserved.
doi:10.1016/j.optlaseng.2008.10.014

needs to calculate the first-order spatial derivatives of the deformed image, consequently, the computational complexity is reduced. Recently, this technique was further simplified and combined with finite element method and 2D generalized cross-validation algorithm for deformation measurement [9].

It should be noted that, in the previous works, the gray level intensity of a physical points in the reference image is assumed as the same in the deformed image. However, in reality, the digital images are sometimes acquired with significant exposure and/or illumination lighting variations during loading [10], moreover, the gain and/or the offset of the imaging device may also change at various time. Obviously, in these cases, the improper assumption of the constant intensity model is prone to produce errors in deformation measurement, and thus is no longer applicable. To overcome this disadvantage of previous spatial-gradient-based algorithms, a more general and practical intensity change model, which takes the possible linear intensity change of the deformed image into consideration, is employed to minimize or eliminate measurement error caused by illumination change and possible significant exposure. Incorporating the displacement mapping function into the intensity change model and followed by Taylor expansions, basic optical flow equation comprising deformation parameter vector is derived. Both linear least squares and iterative least squares (ILS) algorithms can then be used to solve deformation parameters. Calculation using the least squares is exempted from sub-pixel interpolation and iteration, thus it can be implemented with very fast computation speed. However, ILS algorithm providing higher accuracy in the computed displacements and displacement gradients is highly recommended and described in detail. Moreover, the measurements of ILS algorithm are mathematically proved to be equivalent to that of the improved NR method. Nevertheless, the fundamental principle, mathematical derivation and computational process of ILS algorithm are more straightforward and simple, because only first-order spatial derivatives of the deformed image are needed and the concept of correlation criterion is not used.

In mechanical testing and structural stress analysis, full-fields strain distributions are always the most important and valuable information. In view of the large variations in displacement gradients (i.e., strains) directly computed with ILS algorithm or NR method, further data processing technique should be developed so that reliable strain fields can be extracted from the displacement fields. In contrast to the conventional approaches based on smoothing the displacement fields first and followed by differentiation of the smoothed displacement fields [9,11–13], here we propose a simple yet effective pointwise least squares (PLS) algorithm for extracting strain information from the computed displacement fields. To verify the accuracy and effectiveness of the proposed ILS and PLS algorithms for displacement and strain field measurements, two sets of numerical simulation experiments are performed. The results clearly showed that the proposed algorithms can produce accurate measurement both on displacement field and on strain field. Finally, as a practical application, the proposed techniques were used to measure the residual plastic deformation fields of notched GH4169 alloy specimen subjected to tensile fatigue.

2. Displacement field measurement using iterative least squares algorithm

2.1. Intensity change model

Conventional DIC methods resolve deformation parameters by optimizing the predefined correlation criterion. In contrast, the concept of correlation criterion is not used in the iterative spatial-gradient-based method for sub-pixel displacements and displacement gradients measurements. As can be found in previous works [7–9], the fundamental assumption of the method is the gray level intensity of a physical point in the reference image does not change in the deformed image. Thus, the basic equation of optical flow method for the interrogated point (x_i, y_i) is therefore written as

$$f(x_i, y_i) = g(x'_i, y'_i) \quad i = 1, 2, \ldots, n, \tag{1}$$

where $f(x_i, y_i)$ is the grayscale intensity value at point (x_i, y_i) of the reference image; $g(x'_i, y'_i)$ is the grayscale intensity value at point (x'_i, y'_i) of the deformed image; $u(x_i, y_i)$ and $v(x_i, y_i)$ are the displacement components of the point in x and y direction, respectively; n denotes the number of pixels contained in the reference subset.

Obviously, this constant model is hardly valid in practical experimental environment where overexposure/underexposure and non-uniform or unstable illumination as well as the gain and offset of the imaging device usually exist in the digital images acquired at different time. Consequently, a more robust intensity change model should be used to minimize or eliminate measurement error. Here we propose a linear intensity change model, which takes the scale and offset of the intensity into consideration as indicated in Fig. 1.

$$a \times f(x_i, y_i) + b = g(x'_i, y'_i) \quad i = 1, 2, \ldots, n, \tag{2}$$

where a is the scale factor of the intensity change, and b denotes the offset of the intensity change.

It is clear that the previous constant intensity model can be considered as a special case of the present model with $a = 1$ and $b = 0$. Although linear intensity change model is employed here, other non-linear intensity change model can also be easily formulated by simple modification. An example of such modification is $a \times f(x_i,y_i)^2 + bf(x_i,y_i) + c = g(x'_i,y'_i)$ $i = 1,2, \ldots, n$ which involves three constants a, b and c.

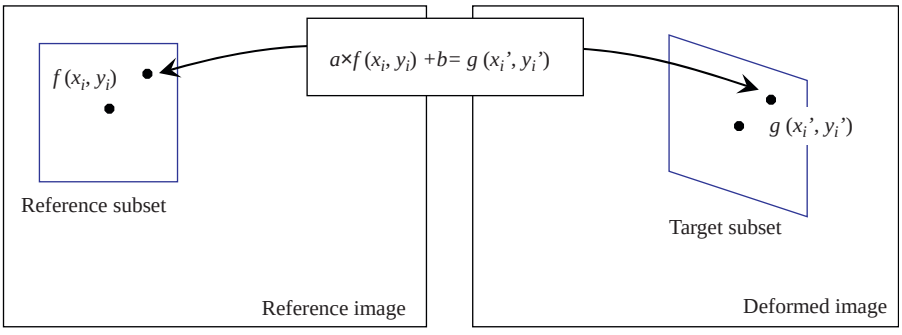

Fig. 1. Schematic figure of the intensity change model for the pixel within the reference subset and the deformed subset.

2.2. Displacement mapping function

It is reasonable to assume that the shape of the reference square subset is changed in the deformed image. Based on the deformation continuity assumption of a deformed solid object, a set of neighboring points in a reference subset should remain as neighboring points in the target subset. If the subset is small enough, the coordinates of the points (x_i, y_j) around the subset center (x, y) in the reference subset can be mapped to the points (x'_i, y'_i) in the target subset according to following displacement mapping function, which allows translation, rotation, shear, normal strains and their combinations of the subset.

$$\begin{aligned} x'_i &= x_i + u + \Delta u + u_x\Delta x_i + u_y\Delta y_i \\ y'_i &= y_i + v + \Delta v + v_x\Delta x_i + v_y\Delta y_i \end{aligned} \tag{3}$$

where Δx and Δy are the distances from the subset center to point (x_i, y_i); u and v are the integer pixel displacement components; Δu and Δv are the sub-pixel displacement components of the reference subset center in x and y directions, respectively; u_x, u_y, v_x, v_y are the first-order displacement gradients of the reference subset. Although only first-order shape function is used in this paper, it is apparent that the below derivation can be easily extended to include both the simplified form of zero-order shape function (translation only) and the more complicated form of second-order shape function [4,6].

$$\mathbf{F}(\mathbf{p}^k) = \begin{bmatrix} g(x_1 + u + \Delta u^k + u_x^k\Delta x_1 + u_y^k\Delta y_1, y_1 + v + \Delta v^k + v_x^k\Delta x_1 + v_y^k\Delta y_1) - a^k f(x_1, y_1) - b^k \\ g(x_2 + u + \Delta u^k + u_x^k\Delta x_2 + u_y^k\Delta y_2, y_2 + v + \Delta v^k + v_x^k\Delta x_2 + v_y^k\Delta y_2) - a^k f(x_2, y_2) - b^k \\ \vdots \\ g(x_n + u + \Delta u^k + u_x^k\Delta x_n + u_y^k\Delta y_n, y_i + v + \Delta v^k + v_x^k\Delta x_n + v_y^k\Delta y_n) - a^k f(x_n, y_n) - b^k \end{bmatrix}$$

2.3. Sup-pixel displacements and displacement gradients calculation using ILS method

Substituting Eq. (3) into Eq. (2), for the ith point within the subset, the following formulation can be obtained:

$$\begin{aligned} &g(x_i + u + \Delta u + u_x\Delta x_i + u_y\Delta y_i, y_i + v + \Delta v + v_x\Delta x_i + v_y\Delta y_i) \\ &\quad - a \times f(x_i, y_i) - b = 0. \end{aligned} \tag{4}$$

By ignoring the second-order and higher-order terms, the Taylor expansions of Eq. (4) at $g(x_i+u, y_i+v)$ yields

$$\begin{aligned} \mathbf{F}_i(\mathbf{p}) = g_i &+ g_{xi}\Delta u + g_{xi}u_x\Delta x_i + g_{xi}u_y\Delta y_i + g_{yi}\Delta v \\ &+ g_{yi}v_x\Delta x_i + g_{yi}v_y\Delta y_i - af_i - b \cong 0, \end{aligned} \tag{5}$$

where $\mathbf{p} = \{\Delta u \quad u_x \quad u_y \quad \Delta v \quad v_x \quad v_y \quad a \quad b\}^T$ denotes the unknown parameter vector containing sub-pixel displacements and displacement gradients of the subset, the scale factor and the offset of the intensity change; g_{xi} and g_{yi} are the x and y directional spatial-gradients of the deformed image at position(x'_i, y'_i), respectively.

For the n $(n>8)$ points within the subset, Eq. (5) can be solved directly using conventional linear least squares with very fast speed as shown in Appendix A. However, the displacement measurement accuracy can be increased considerably using the following iterative least squares algorithm.

The non-linear function $\mathbf{F}(\mathbf{p})$ can be optimized using Newton iteration scheme,

$$\mathbf{F}_i(\mathbf{p}^{k+1}) = \mathbf{F}_i(\mathbf{p}^k) + \nabla\mathbf{F}_i(\mathbf{p}^k)(\mathbf{p}^{k+1} - \mathbf{p}^k) = 0 \tag{6}$$

where $\mathbf{p}^{k+1}$, $\mathbf{p}^k$ are the solutions of $(k+1)$th and kth round iteration, respectively,

$$\nabla\mathbf{F}_i(p^k) = [g_{xi}\Delta x_i g_{xi}\Delta y_i g_{xi} g_{yi}\Delta x_i g_{yi}\Delta y_i g_{yi} - f_i - 1]$$

and

$$\begin{aligned} \mathbf{F}_i(p^k) = [&g(x_i + u + \Delta u^k + u_x^k\Delta x_i + u_y^k\Delta y_i, y_i + v \\ &+ \Delta v^k + v_x^k\Delta x_i + v_y^k\Delta y_i) - a^k f(x_i, y_i) - b^k]. \end{aligned}$$

For the $i = 1,2, \ldots, n$ $(n>8)$ points, we get n equations of Eq. (6). Thus, the iterative least squares approximation solution to this equation can be written as

$$\mathbf{p}^{k+1} = \mathbf{p}^k - [\nabla\mathbf{F}(\mathbf{p}^k)^T\nabla\mathbf{F}(\mathbf{p}^k)]^{-1}\nabla\mathbf{F}(\mathbf{p}^k)^T\mathbf{F}(\mathbf{p}^k), \tag{7}$$

where

$$\nabla\mathbf{F}(\mathbf{p}^k) = \begin{bmatrix} g_{x1} & \Delta x_1 g_{x1} & \Delta y_1 g_{y1} & g_{y1} & \Delta x_1 g_{y1} & \Delta y_1 g_{y1} & -f_1 & -1 \\ g_{x2} & \Delta x_2 g_{x2} & \Delta y_2 g_{y2} & g_{y2} & \Delta x_2 g_{y2} & \Delta y_2 g_{y2} & -f_2 & -1 \\ \vdots & \vdots & \vdots & \vdots & \vdots & \vdots & \vdots & \vdots \\ g_{xn} & \Delta x_n g_{xn} & \Delta y_n g_{yn} & g_{yn} & \Delta x_n g_{yn} & \Delta y_n g_{yn} & -f_n & -1 \end{bmatrix}$$

It is important to mention that the present ILS algorithm is actually equivalent to the optimization of a new sum of squared difference (SSD) correlation criterion using improved NR method as proved in Appendix B. Nevertheless, the fundamental principle, mathematical derivation and computational process of ILS algorithm are more straightforward and simple, because only first-order spatial derivatives of the deformed image are needed and the concept of correlation criterion is not used.

2.4. Initial estimate of iteration

It should be noted that initial estimate of the parameter vector must be provided prior to an iterative process. In this work, the integral-pixel displacements obtained by direct spatial domain searching scheme are used as the initial estimation of iteration. After the integral-pixel displacement (u, v) at point (x, y) in reference image is obtained, the initial estimate of Newton's iteration can be given as $\mathbf{p}^0 = (0, 0, 0, 0, 0, 0, 1, 0)^T$. It is worth noting that in certain special cases where large relative rotation and/or deformation exists between the reference and deformed image, the simple integer displacement searching scheme is not able to produce a reasonable result, thus, some new techniques [14] should be used to provides reliable initial estimate of the deformation.

2.5. Bicubic spline interpolation

It is evident that, during the process of iteration, gray value $g(x'_i, y'_i)$ and its gradients $g_x(x'_i, y'_i)$, $g_y(x'_i, y'_i)$ must be provided. Because the coordinates of points in deformed subset can assume sub-pixel values and no gray level information is available between pixels in digital images, therefore, an interpolation scheme is needed in the realization of the above iterative method. In this study, a bicubic spline interpolation scheme [15] is implemented to determine the gray

values and first-order gray gradients at sub-pixel locations as follows:

$$g(x,y)=\sum_{m=0}^{3}\sum_{n=0}^{3}\alpha_{mn}x^m y^n. \tag{8}$$

The unknown coefficients in Eq. (8) can be determined by the gray intensity of an interpolation area of given points (6×6 pixels in this study) and the continuity requirements. As will be seen, using the bicubic spline interpolation scheme, the program shows high registration accuracy and well convergence character.

2.6. Convergence conditions

The convergence conditions were set to ensure that variations in sub-pixel displacements Δu and Δv were equal to or less than 10^{-4} pixel and variations in displacement gradients were equal to or less than 5×10^{-6} (i.e., 5 με).

3. Strain field measurement using pointwise least squares algorithm

3.1. Strain field estimation techniques

Although the displacement gradients (i.e., strains) can be directly calculated using the ILS algorithm, large variations in the calculated results indicated that they cannot be directly used as reliable strain measurement. Alternatively, strains can also be computed from numerical differentiation of the estimated displacement field. However, numerical differentiation will

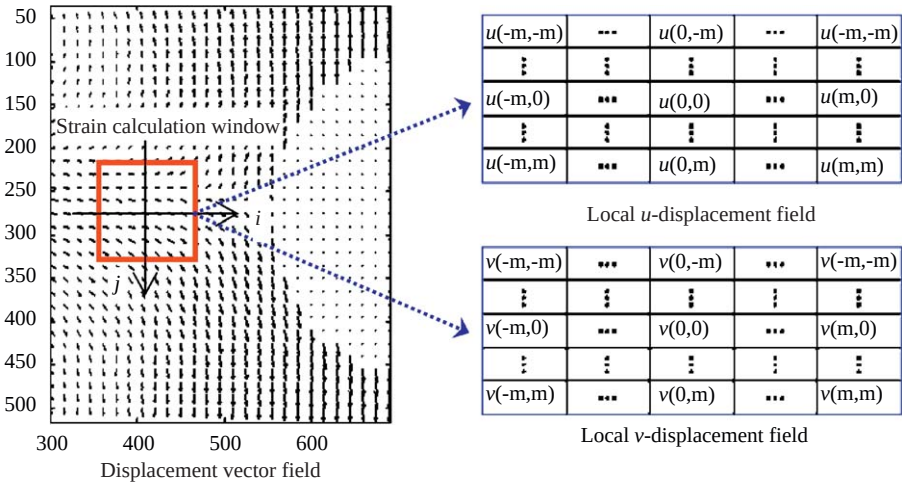

Fig. 2. Principle of the PLS algorithm for full-field strain estimation.

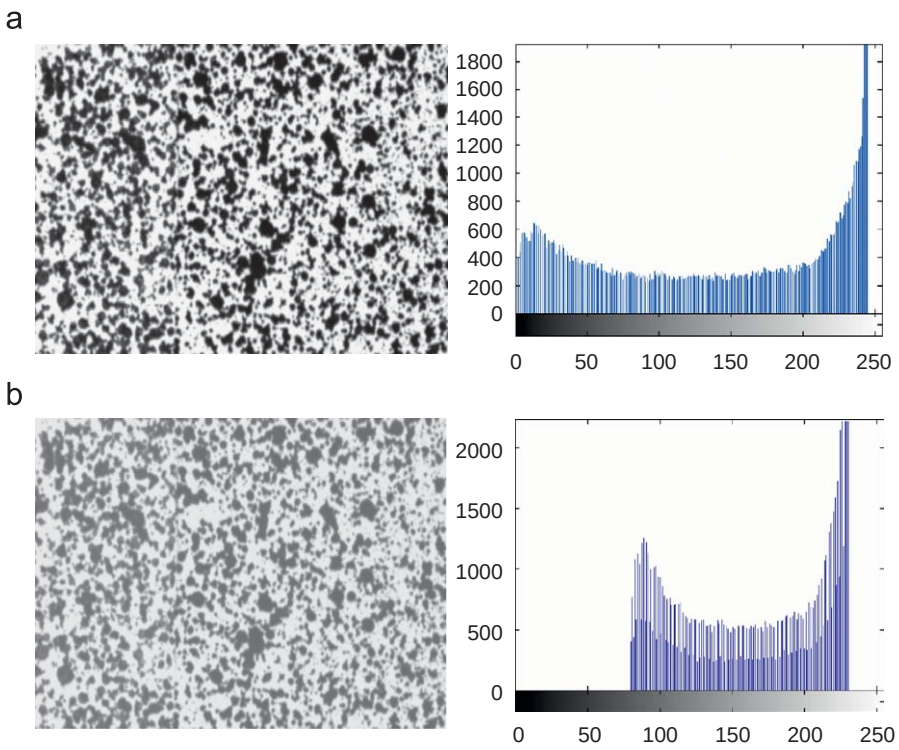

Fig. 3. Reference image, deformed image and their histograms.

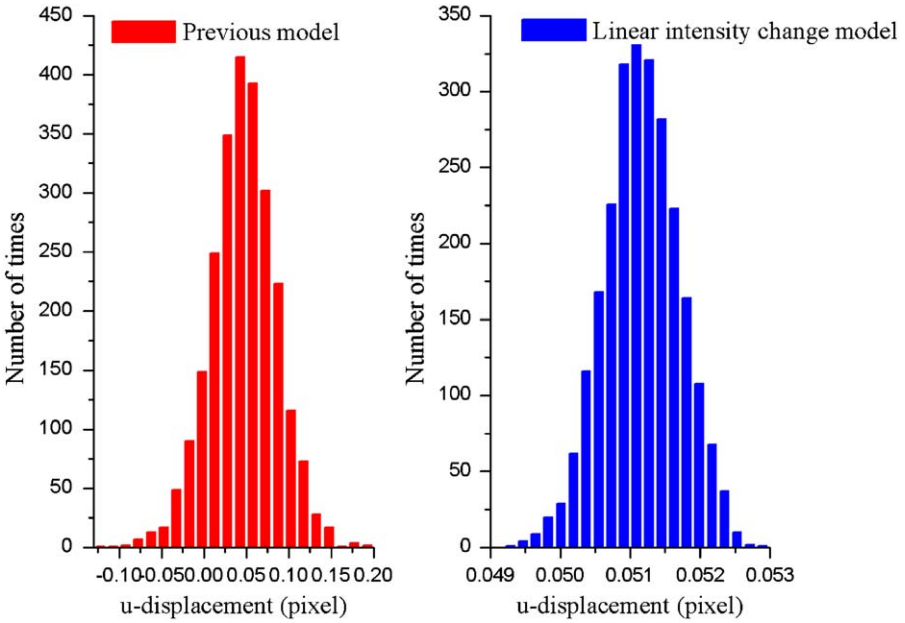

Fig. 4. Histograms of the measured u-displacements by ILS method with different intensity change model.

Table 1
Measured u-displacements by ILS method with different intensity change model ($u = 0.05$ pixels).

Intensity change model	Average	Standard deviation	Minimum	Maximum	Average iterations
Constant model	0.0464	0.0388	−0.1211	0.1910	7.738
Linear change model	0.0512	0.0005	0.0493	0.0529	2.187

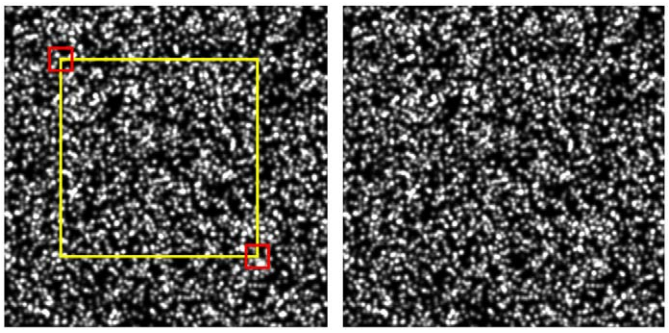

Fig. 5. Reference image (left) and deformed image (right), the yellow rectangular of the left image is calculation area, and the red square is the 41 × 41 pixels subset used for correlation analysis.

amplify the noise contained in the displacements. Thus, it is widely accepted by many researchers that smoothing the computed displacement fields first and followed by differentiation would improve the strains calculation with heightened accuracy. This led to a number of techniques that had been introduced, such as finite element smoothing [9,11], thin plate spline smoothing [12] and other smoothing algorithms [13]. However, the smoothing of noisy discrete data using penalty finite element method or thin plate spine is quite cumbersome. A pointwise local least squares fitting technique described in the following subsection would be a more practical approach for strain estimation.

3.2. Pointwise least squares for strain estimation

The implementation of local least squares fitting technique for strain estimation can be explained as follows. As shown in Fig. 2, in order to compute the strains of current point, we first select a square window containing $(2m+1)\times(2m+1)$ discrete points (i.e., strain calculation window) around it. If the strain calculation window is small enough, the displacement distributions in it can be approximated as a linear plane, thus we have

$$\begin{aligned} u(i,j) &= a_0 + a_1 x + a_2 y \\ v(i,j) &= b_0 + b_1 x + b_2 y \end{aligned} \tag{9}$$

where $i, j = -m: m$ are the local coordinates within the strain calculation window, $u(i,j)$ and $v(i,j)$ are the original displacements at location (i, j) obtained by DIC as indicated in Fig. 2, and $a_{i=0,\,1,\,2}$, $b_{i=0,\,1,\,2}$ are the unknown polynomial coefficients to be determined.

Eq. (9) can be rewritten into the form of matrix. For instance, the first formulation of Eq. (9) can be rewritten as

$$\begin{bmatrix} 1 & -m & -m \\ 1 & -m+1 & -m \\ \vdots & \vdots & \vdots \\ 1 & 0 & 0 \\ \vdots & \vdots & \vdots \\ 1 & m-1 & m \\ 1 & m & m \end{bmatrix} \begin{pmatrix} a_0 \\ a_1 \\ a_2 \end{pmatrix} = \begin{Bmatrix} u(-m,-m) \\ u(-m+1,-m) \\ \vdots \\ u(0,0) \\ \vdots \\ u(m-1,m) \\ u(m,m) \end{Bmatrix} \tag{10}$$

Thus, simple linear least squares method can be used to solve the unknown polynomial coefficients. The desired Cauchy

strains or Green strains at the center point of local sub region can therefore be computed based on the obtained coefficients $a_{i=0,1,2}$, $b_{i=0,1,2}$. Since the noises can be largely removed in the process of local fitting, the accuracy of the calculated strains would be greatly improved.

It is quite important to note that, for those points located in the vicinity of calculation area boundaries or discontinuity area, the strain calculation window around which may contain less than $(2m+1)\times(2m+1)$ points. To obtain the strains of these points, a continuity extension of the displacement field at the calculation area boundaries was performed by Wattrisse et al. [16]. In this paper, a more simple yet effective data reduction technique is proposed. Considering the valid points within the calculation area can be easily labeled and identified, thus those invalid points within the local strain calculation window can also be distinguished and exclude from the local least squares fitting. The data reduction is reasonable because generally the used strain calculation window incorporates more than one hundred points, while Eq. (9) contains only three unknown parameters.

3.3. Selection of strain calculation window size

It is quite important to note that, to obtain reasonable and accurate full-field strain estimation using PLS method, the following two aspects are important and should be considered. One is the accuracy of displacement fields obtained by DIC, and the other is the size of the local strain calculation window used for pointwise least squares fitting. For homogeneous deformation, a large strain calculation window is preferred. However, for inhomogeneous deformation, a proper size of strain calculation window should be selected with care to get a trade-off between strain accuracy and smoothness. Because a small strain calculation window cannot suppress the noise of the displacements, while a large strain calculation window may lead to the unreasonable linear approximation of deformation within the strain calculation window. Normally, the size of strain calculation window can be selected between 11×11 to 21×21 points according to our experiences.

4. Verification using numerical experiments

To investigate the performance of ILS algorithm for displacement measurement and PLS method for strain estimation, two sets of numerical simulation experiments were conducted in this study. Instead of using actual experiments, numerical simulation experiment were used for the purpose of isolating the possible errors caused by the image acquisition system, such as the camera lens distortion, imperfect loading as well as out-of-plane displacement of the specimen.

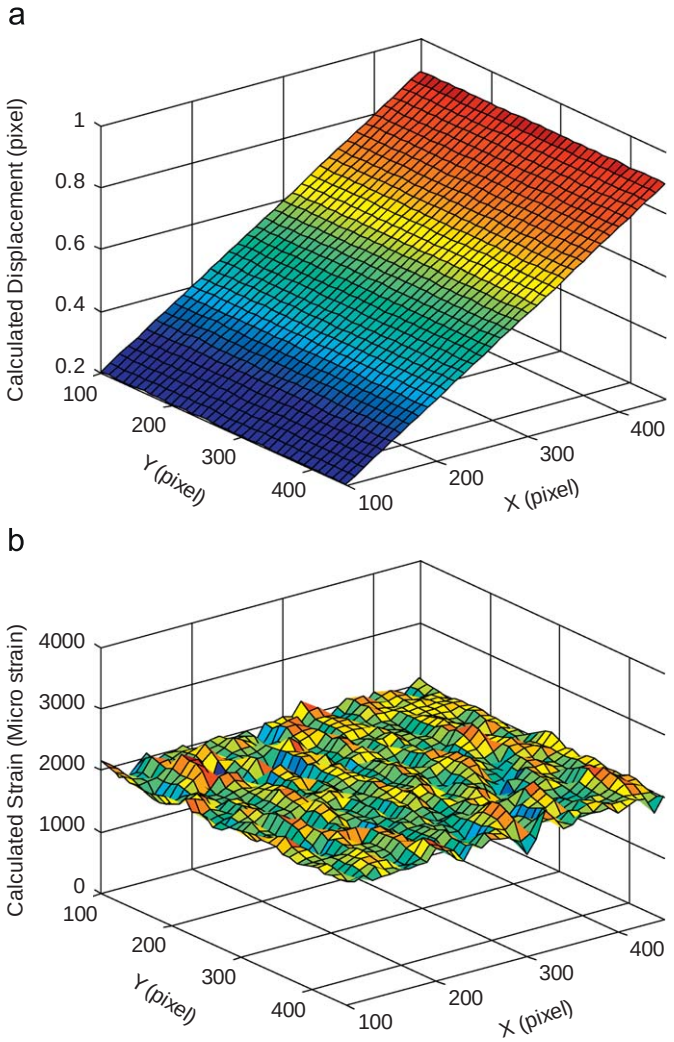

Fig. 6. The displacement field (a) and strain field (b) in *x*-direction obtained by ILS method.

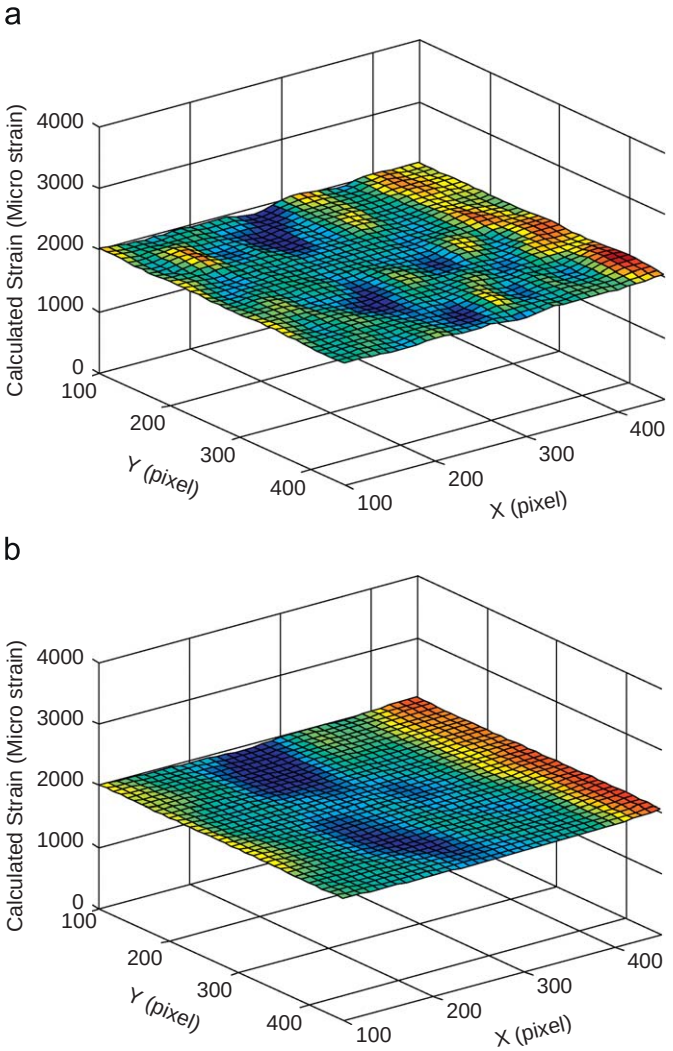

Fig. 7. The strain field obtained by PLS algorithm with (a) 11×11 points, and (b) 21×21 points strain calculation window.

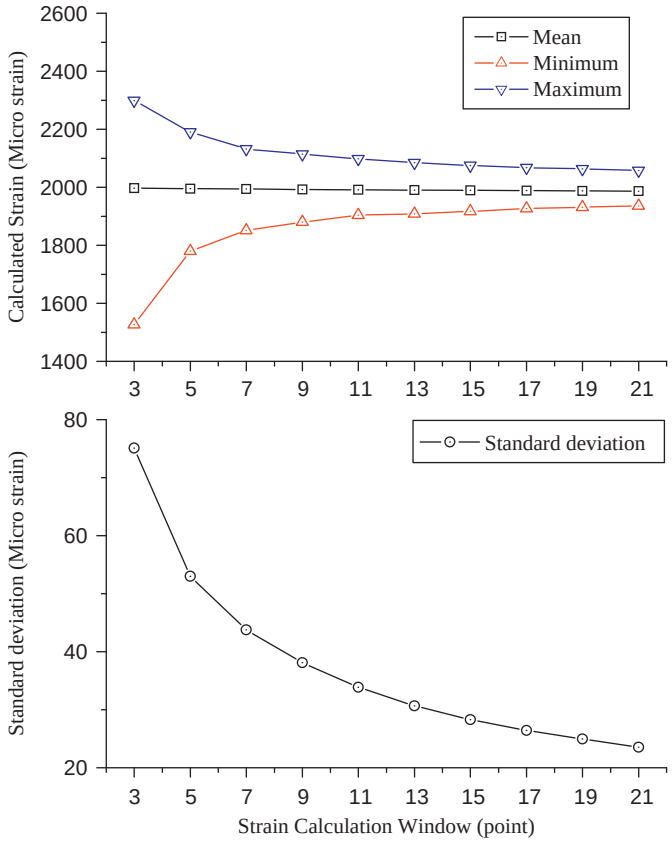

Fig. 8. The calculated strain of homogeneous deformation by PLS algorithm with various strain calculation window.

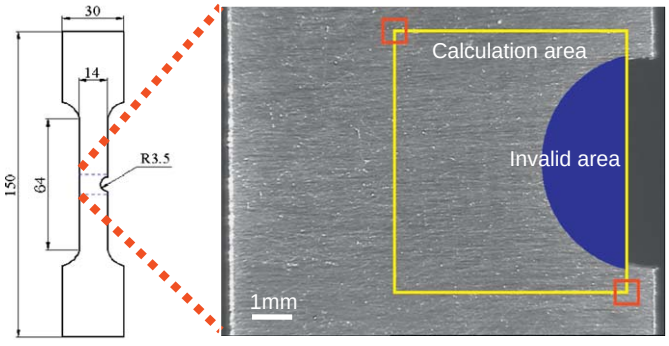

Fig. 9. Geometry of the specimen and the reference image: the rectangular area of the left image is calculation area, and the invalid area to avoid calculation is labeled with blue color.

4.1. Verification of ILS algorithm for displacement field measurement

The first validation experiment was conducted to evaluate the performance of the ILS method. An 8-bit speckle pattern image of 768×576 pixels taken from our previous actual experiment was used as the reference image. Afterwards, the reference speckle image was first shifted 0.05 pixels in x-direction according to shift theorem, then the shifted image was further artificially adjusted with 50% increase in brightness and 80% increases in contrast to simulate practical illumination lighting changes or the gain and offset of the camera, and was taken as deformed image. These two images and their histogram are shown in Fig. 3, which clearly show the variations in image appearance.

The displacements of the translated speckle pattern were computed at regularly distributed $2501 (= 61 \times 41)$ points (the distance between neighboring points is 10 pixels and the subset used is 31×31 pixels) using the ILS algorithm with the constant intensity model adopted in the previous works and the present linear intensity change model. Fig. 4 and Table 1 give the histograms and statistical results of the computed u-displacements, respectively. Although the statistical distributions of the measured displacements as shown in Fig. 4 are very similar, the displacements measured with proposed model however are located within a more narrow range. It is evident that the proposed linear intensity change model is insensitive to the variations in illumination condition, and the ILS method using the proposed model provides more accurate measurement with much less average iterations, approximately 1/4 of that for the previous model. This clearly showed the effectiveness of the proposed method.

4.2. Verification of LS algorithm for strain field measurement

In the second validation experiment, numerical uniaxial tensile test was performed to verify the performance of the PLS algorithm for strain field estimation. The reference speckle image and the deformed speckle image, as shown in Fig. 5(a) and (b), are generated using the simulation algorithm proposed by Zhou and Goodson [7]. The pre-assigned homogenous strain is 2000 με in x-direction of the image. Detailed features of the simulated speckle image are: the size of simulated images is 576×576 pixels; the size of speckles is 4 pixels; the number of speckle granules is 4000.

Fig. 6 shows the displacement and strain fields in x-direction at 5041 locations on a 71×71 grid directly computed by ILS method with a subset of 41×41 pixels. It can be seen from Fig. 6(a) that the calculated displacement field agrees well with the pre-assigned linear distribution. However, as indicated in Fig. 6(b), the directly obtained strain field is highly oscillatory with

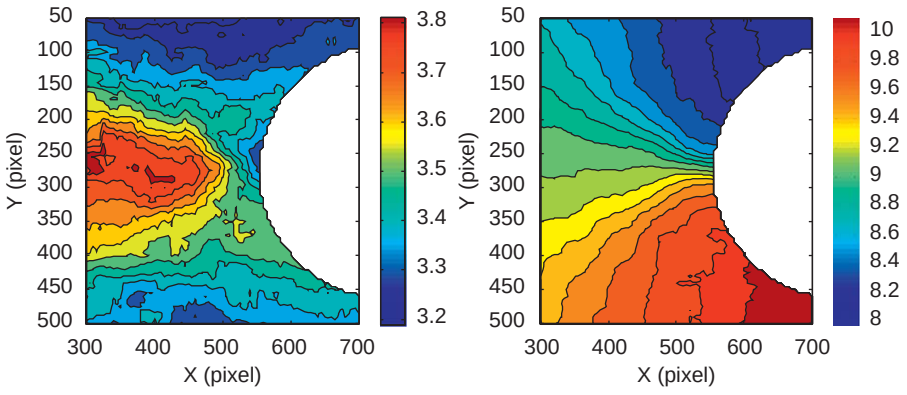

Fig. 10. Displacement fields obtained by ILS method: (a) u-displacement field, and (b) v-displacement field.

standard deviation of 300 microstrain. Thus, it cannot be directly used as reliable local strain estimation.

By contrast, the strain fields obtained by use of the PLS method with 11×11 and 21×21 points strain calculation window are exhibited in Fig. 7(a) and (b) respectively. As the actual strain is a constant value in the calculation area, we can clearly observe that the strain fields obtained by PLS method agree well with the pre-assigned one. Besides, it is also clear that small strain calculation window produces large variations in the computed strains.

Fig. 8 shows the maximum, minimum, mean value and standard derivation of strains obtained by PLS algorithm with strain calculation window varying from 3×3 to 21×21 points. It can be found in Fig. 8 that although the mean strain values are all close to the pre-assigned one, the standard deviation of strain using larger strain calculation window decreases obviously. Because large-strain calculation window incorporates more points, the ability to suppress noise will be more robust and the resulting strain filed will be smoother. It means that the accuracy of the strain measurement increases with the use of larger strain calculation window size in the case of homogeneous deformation.

5. Application of ILS and PLS for residual plastic deformation measurement

The ILS and PLS algorithms were also used to determine the residual plastic deformation of a notched GH4169 alloy specimen subjected to tensile fatigue. The geometry of the specimen is shown in the left side of Fig. 9. It is a tensile specimen with a semicircle-shaped notch in the middle of right side of the specimen. GH4169 nickel-based alloy has been widely used as a high-temperature resistant structural material in aircraft engine. The aim of the experiment is to investigate the plastic strain evolution process of the specimen with respect to applied fatigue cycles. After polished by sand paper, the random gray-level distribution of the specimen surface can be used as the characteristics for correlation matching. The fatigue test was performed in a material testing machine (MTS 810) with loading direction along the rolling direction. The specimen was tightly clamped at both ends with its bottom fixed. The movable upper clamper stretches the specimen with cyclic loading of $0 \rightarrow 10.5\,\mathrm{KN} \rightarrow 0$ at a frequency of 10 Hz. Cold white light source was used to illuminate the specimen during fatigue test. After the specimen was clamped tightly on the material testing machine, a clear image of the specimen surface was captured as the reference image. The deformed image was taken after 26,000 fatigue cycles. The recorded 8-bit digital images had a size of 768×576 pixels and a corresponding spatial resolution of 0.02 mm per pixel.

The selected calculation area is indicated in Fig. 9, and the two key parameters used in DIC analysis, i.e., the subset size is chosen as 41×41 pixels, and the step size (distance between neighboring points) is chosen as 5 pixels, respectively. Note that the specimen surface contains a semicircle-shaped notch, which was labeled as invalid area to avoid calculation as shown in the right side of Fig. 9. The image pairs of the specimen surface were analyzed using the ILS algorithm first, and the displacement fields were shown in Fig. 10.

Then, the computed displacement fields were fitted locally using the PLS method to compute strain fields. The strain calculation window is chosen as 15×15 points (corresponds to a local image area of 71×71 pixels). The computed normal strain in x and y direction as well as the shear strain were presented in Fig. 11, from which we can see that the apparent strain concentrations appear at the root of the notch.

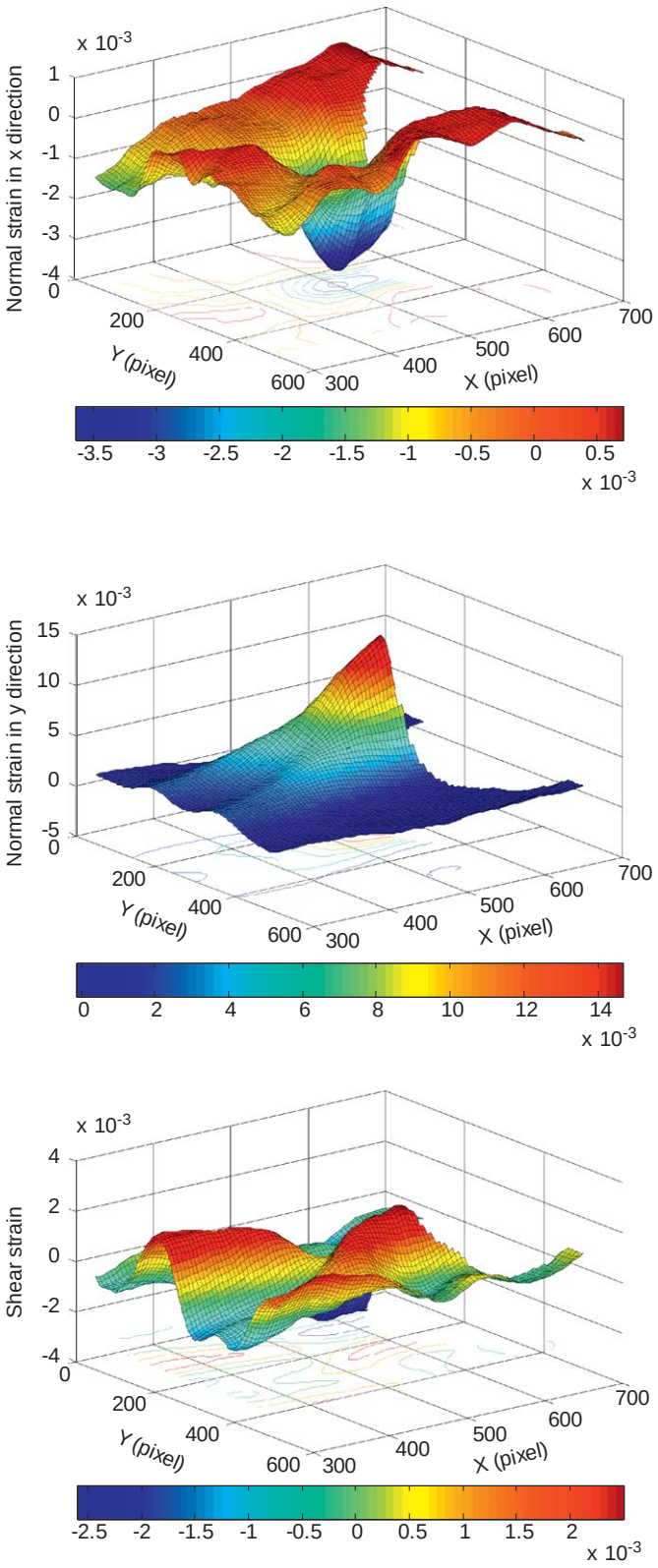

Fig. 11. Residual plastic strain fields computed by PLS fitting of the displacement fields.

6. Discussion and conclusion

It is well-known that the zero-mean normalized cross-correlation (ZNCC) function or the zero-mean normalized sum of squared difference (ZNCC) function is also insensitive to the

linear intensity change of the deformed image as proved in our previous work [5,6]. However, we should note that the optimization of ZNCC or ZNSSD correlation function using NR method is more complicated than the proposed spatial-gradient-based method using ILS algorithm. Because for the optimization of ZNCC or ZNSSD correlation function using the classic NR method, the mean value and standard deviation of the subset intensity as well as the second-order derivatives of correlation function (i.e., Hessian matrix) must be computed as indicated in Ref. [5], while the proposed method only needs to calculate the first-order spatial derivatives of the deformed image.

In this paper, a more robust intensity change model based on optical flow method is developed. It takes into account the linear change in intensity during digital image acquisition and various displacement mapping functions can be easily incorporated into the model. An ILS algorithm is recommended to resolve displacements and displacement gradients. Although conventional linear least squares algorithm can also be used for calculation of displacements and displacement gradients with very fast computation speed, its accuracy is lower than that of ILS algorithm. While the proposed ILS algorithm is mathematically proved to be equivalent to the improved NR method, the fundamental principle and mathematical derivation is more straightforward and simple. To extract reliable strain fields from the already computed displacement fields, PLS algorithm is utilized. Simple data reduction technique for the points located at discontinuity areas is also addressed. Using the proposed algorithms, the computation of deformation fields using DIC method is simpler and more straightforward than the previous techniques that combined the NR method and finite element smoothing.

Appendix A. deformation parameters calculation using conventional least squares

Sup-pixel displacements and displacement gradients can be calculated using conventional linear least squares approximation. Eq. (4) can be written as

$$g_{xi}\Delta u + g_{xi}u_x\Delta x_i + g_{xi}u_y\Delta y_i + g_{yi}\Delta v + g_{yi}v_x\Delta x_i + g_{yi}v_y\Delta y_i - af_i - b = -g_i \tag{11}$$

For the $i = 1,2,\ldots,n = (2m+1)\times(2m+1)$ pixels within the interrogated subset, Eq. (11) can be rewritten into a matrix form,

$$\mathbf{Xp} = \mathbf{B} \Leftrightarrow \begin{bmatrix} g_{x1} & x_1g_{x1} & y_1g_{y1} & x_1g_{y1} & y_1g_{y1} & g_{y1} & -f_1 & -1 \\ g_{x2} & x_2g_{x2} & y_2g_{y2} & x_2g_{y2} & y_2g_{y2} & g_{y2} & -f_2 & -1 \\ \vdots & \vdots & \vdots & \vdots & \vdots & \vdots & \vdots & \vdots \\ g_{xn} & x_ng_{xn} & y_ng_{yn} & x_ng_{yn} & y_ng_{yn} & g_{yn} & -f_n & -1 \end{bmatrix} \times \begin{pmatrix} \Delta u \\ u_x \\ u_y \\ \Delta v \\ v_x \\ v_y \\ a \\ b \end{pmatrix} = \begin{pmatrix} -g_1 \\ -g_2 \\ \vdots \\ -g_n \end{pmatrix} \tag{12}$$

Thus, the solution of the overdetermined equation, i.e., desired deformation parameter vector, can be computed using conventional linear least squares.

$$\mathbf{p} = (\mathbf{X}^T\mathbf{X})^{-1}\mathbf{X}^T\mathbf{B} \tag{13}$$

Since the calculation doesn't require sub-pixel interpolation and iteration, it can be implemented with very fast computation speed. But the accuracy is lower than that of the ILS algorithm, because the solution of linear least squares can be considered as the first iteration solution of ILS algorithm.

Appendix B. relations of ILS algorithm to improved NR method

We will prove that the ILS algorithm is actually equivalent to the optimization of the following sum of squared difference (SSD) correlation function using improved Newton–Raphson method with an approximation to the Hessian matrix as proposed by Vendroux and Knauss [3]. First, we write the corresponding SSD correlation function as follows:

$$C_{SSD}(\mathbf{p}) = \sum_{i=1}^{n}[g(x_i + u(x_i,y_i), y_i + v(x_i,y_i)) - a\times f(x_i,y_i) - b]^2 \tag{14}$$

Similarly, $\mathbf{p} = \{\Delta u \quad u_x \quad u_y \quad \Delta v \quad v_x \quad v_y \quad a \quad b\}^T$ represents the unknown parameter vector.

When the reference and target subsets get their maximum similarity, the minimum C($\mathbf{p}$) is reached. In other words, the gradient of C($\mathbf{p}$) must converge to zero, then, we have

$$\nabla C(\mathbf{p}) = \left(\frac{\partial C}{\partial p_j}\right)_{j=1,\ldots,8} = 0 \tag{15}$$

The Newton–Raphson method can be used to solve for roots of Eq. (15). The NR equation can be correspondingly written as

$$\nabla C(\mathbf{p}^{k+1}) = \nabla C(\mathbf{p}^k) + \nabla\nabla C(\mathbf{p}^k)(\mathbf{p}^{k+1} - \mathbf{p}^k) = 0 \tag{16}$$

where $\nabla C(\mathbf{p}^k)$ is the first-order derivative of the correlation function and is of the following form:

$$\nabla C(\mathbf{p}^k) = \left(\frac{\partial C(\mathbf{p}^k)}{\partial p_i}\right)_{i=1,\ldots,8} = 2\sum_{i=1}^{N}[g(x'_i,y'_i) - a\times f(x_i,y_i) - b]\begin{pmatrix} g_{xi} \\ \Delta x_ig_{xi} \\ \Delta y_ig_{xi} \\ g_{yi} \\ \Delta x_ig_{yi} \\ \Delta y_ig_{yi} \\ -f_i \\ -1 \end{pmatrix} \tag{17}$$

$\nabla C(\mathbf{p}^k)$ is the second-order derivative of the correlation function, also called Hessian matrix. It can be written as

$$\nabla\nabla C(\mathbf{p}^k) = \left(\frac{\partial^2 C(\mathbf{p}^k)}{\partial p_i \partial p_j}\right)_{\substack{i=1,\ldots,8 \\ j=1,\ldots,8}} \tag{18}$$

If $\mathbf{p}^k$ is close to the exact solution, we have $g(x'_i, y'_i) - a\times f(x_i, y_i) - b \cong 0$. Thus, it is reasonable to drop the first part of Hessian matrix. Then, the approximation of Hessian matrix can be written as

$$\nabla\nabla C(\mathbf{p}^k) \cong 2\sum_{i=1}^{N}\left[(g_{xi}\Delta x_ig_{xi}\Delta y_ig_{xi}g_{yi}\Delta x_ig_{yi}\Delta y_ig_{yi} - f_i - 1)\begin{pmatrix} g_{xi} \\ \Delta x_ig_{xi} \\ \Delta y_ig_{xi} \\ g_{yi} \\ \Delta x_ig_{yi} \\ \Delta y_ig_{yi} \\ -f_i \\ -1 \end{pmatrix}\right] \tag{19}$$

Rearrange Eq. (16), we get

$$\mathbf{p}^{k+1} = \mathbf{p}^k - (\nabla\nabla C(\mathbf{p}^k))^{-1}\nabla C(\mathbf{p}^k). \quad (20)$$

Compared with Eq. (7), it can be easily found that $2 \times (\nabla \mathbf{F}(\mathbf{p}^k)^T \mathbf{F}(\mathbf{p}^k)) = \nabla\nabla C(\mathbf{p}^k)$ $2 \times (\nabla \mathbf{F}(\mathbf{p}^k)^T \nabla \mathbf{F}(\mathbf{p}^k)) = \nabla\nabla C(\mathbf{p}^k)$. Thus, the solutions of Eqs. (7) and (20) are completely identical.

References

[1] Pan B, Xie HM, Xu BQ, et al. Performance of sub-pixel registration algorithms in digital image correlation. Meas Sci Technol 2006;17(6):1615–21.

[2] Bruck HA, McNeil SR, Sutton MA, Peters WH. Digital image correlation using Newton–Raphson method of partial differential correction. Exp Mech 1989; 29(3):261–7.

[3] Vendroux G, Knauss WG. Submicron deformation field measurements: part2. Improved digital image correlation. Exp Mech 1998;38(2):86–92.

[4] Lu H, Cary PD. Deformation measurement by digital image correlation: implementation of a second-order displacement gradient. Exp Mech 2000;40(4):393–400.

[5] Pan B, Xie HM, Guo ZQ, Hua T. Full-field strain measurement using a two-dimensional Savitzky–Golay digital differentiator in digital image correlation. Opt Eng 2007;46(3):033601.

[6] Pan B, Xie HM, Gao JX, Asundi A. Improved speckle projection profilometry for out-of-plane shape measurement. Appl Opt 2008;47(29):5527–33.

[7] Zhou P, Goodson KE. Subpixel displacement and deformation gradient measurement using digital image/speckle correlation. Opt Eng 2001;40(8): 1613–20.

[8] Davis CQ, Freeman DM. Statistics of subpixel registration algorithms based on spatiotemporal gradients or block matching. Opt Eng 1998;37(4):1290–8.

[9] Meng LB, Jin GC, Yao XF. Application of iteration and finite element smoothing technique for displacement and strain measurement of digital speckle correlation. Opt Lasers Eng 2007;45:57–63.

[10] Tong W. An evaluation of digital image correlation criteria for strain mapping applications. Strain 2005;41(4):167–75.

[11] Sutton MA, Turner JL, Bruck HA, Chao TA. Full-field representation of discretely sampled surface deformation for displacement and strain analysis. Exp Mech 1991;31(2):168–77.

[12] Wang CCB, Deng JM, Ateshian GA, et al. An automated approach for direct measurement of two-dimensional strain distributions within articular cartilage under unconfined compression. J Biomechanical Eng Trans ASME 2002;124(5):557–67.

[13] Tong W. Detection of plastic deformation patterns in a binary aluminum alloy. Exp Mech 1997;37(4):452–9.

[14] Pan B, Xie H, Xia Y, Wang Q. Large deformation measurement based on reliable initial guess in digital image correlation method. Acta Optica Sinica 2009;29(2):212–9 (in Chinese).

[15] Press, William H. C+ Numerical Algorithms. Beijing: Publishing House of Electronics Industry; 2003.

[16] Wattrisse BC, Muracciole A, Nemoz-Gaillard JM. Analysis of strain localization during tensile tests by digital image correlation. Exp Mech 2001; 41(1):29–39.